AD-A070 594 MARYLAND UNIV COLLEGE PARK DEPT OF PHYSICS AND ASTRONOMY F/G 20/5
CYCLOTRON MASER INSTABILITY FOR INTENSE SOLID ELECTRON BEAMS,(U)
1975 H UHM, R C DAVIDSON N00014-75-C-0309

UNCLASSIFIED NL

| OF |
AD
A070594

END
DATE
FILMED
8-79
DDC

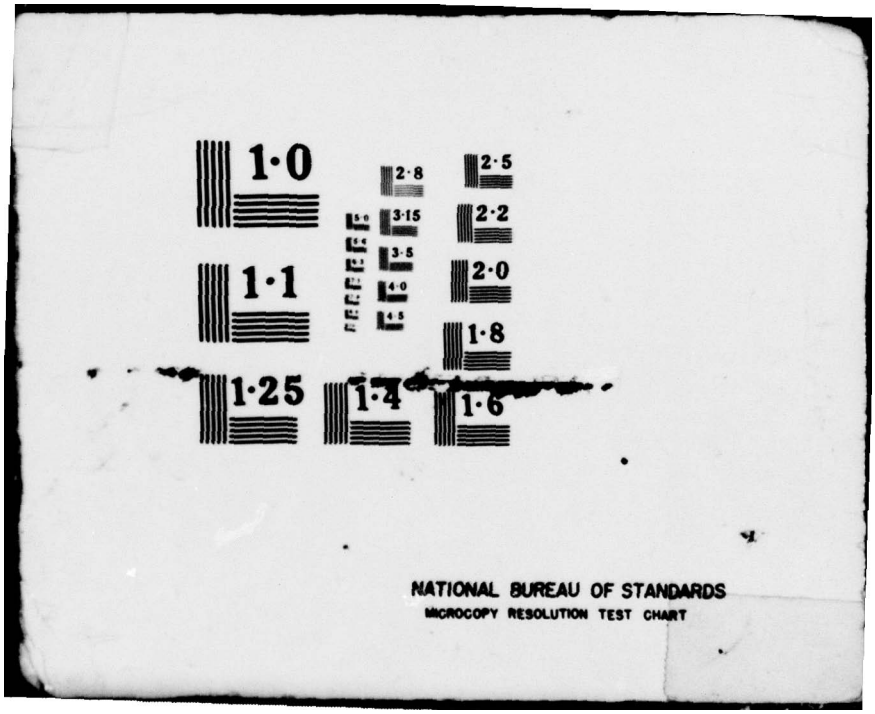
1·0
1·1
1·25
2·8
3·15
3·5
4·0
1·4
2·5
2·2
2·0
1·8
1·6
NATIONAL BUREAU OF STANDARDS
MICROCOPY RESOLUTION TEST CHART

DDC PROCESSING DATA

PHOTOGRAPH THIS SHEET

RETURN TO DDA-2 FOR FILE

II
LEVEL

1
INVENTORY

AD A070594
DDC ACCESSION NUMBER

Cyclotron Maser Instability for Intense Solid---
Uhm, Davidson
DOCUMENT IDENTIFICATION

DISTRIBUTION STATEMENT A
Approved for public release;
Distribution Unlimited

DISTRIBUTION STATEMENT

Accession For
NTIS GRA&I
DDC TAB
Unannounced
Justification
By
Distribution/
Availability Codes
Dist. | Avail and/or special
A

DISTRIBUTION STAMP

DDC
RECEIVED
JUN 28 1979

DATE ACCESSIONED

79 06 27 319

DATE RECEIVED IN DDC

PHOTOGRAPH THIS SHEET

RETURN TO DDA-2

Code 6702

CYCLOTRON MASER INSTABILITY FOR INTENSE SOLID ELECTRON BEAMS

Han S. Uhm
Department of Physics and Astronomy
University of Maryland
College Park, Maryland 20742

and

Ronald C. Davidson*
Office of Fusion Energy
Department of Energy
Washington, D. C. 20545

1975

The cyclotron maser instability for a solid relativistic electron beam propagating parallel to a uniform axial magnetic field $B_0\hat{e}_z$ is investigated. The stability analysis is carried out within the framework of the linearized Vlasov-Maxwell equations. It is assumed that $\nu/\hat{\gamma}<<1$, where ν is Budker's parameter and $\hat{\gamma}mc^2$ is the electron energy. Stability properties are investigated for the choice of equilibrium distribution function in which all electrons have the same value of total perpendicular energy, the same value of axial velocity, and a step-function distribution in canonical angular momentum. The instability growth rate is calculated including a determination of the optimum value of the beam radius R_0 for maximum growth. It is found that the maximum growth rate for a solid beam is comparable to the maximum growth rate for a hollow beam.

Work on this report was supported by ONR Contract N00014-75-C-0309 and/or N00014-67-A-0239 monitored by NRL 6702. 02.

*On leave of absence from the University of Maryland, College Park, Maryland 20742

I. INTRODUCTION

In recent years, the cyclotron maser instability[1-9] has been extensively investigated with particular emphasis on the implications for intense microwave generation. For the most part, previous theoretical analyses of this instability have been carried out for hollow electron beams.[6-9] The present paper examines the equilibrium and cyclotron maser stability properties of a solid relativistic electron beam within the framework of the linearized Vlasov-Maxwell equations, including a determination of the optimum value of the beam radius R_0 for maximum growth rate.

The present analysis is carried out for an infinitely long electron beam propagating parallel to a uniform axial magnetic field $B_0\hat{e}_z$. Equilibrium and stability properties are calculated for the specific choice of electron distribution function [Eq. (3)],

$$f_e^0(H,P_\theta,P_z) = \frac{n_0}{2\pi\gamma_0 m}\,\delta(H_\perp-\gamma_0 mc^2)\Theta(P_\theta-P_0)\delta(P_z-\hat{\gamma}mV_z) ,$$

where $H_\perp$ is the perpendicular energy, P_θ is the canonical angular momentum, P_z is the axial canonical momentum, $\Theta(x)$ is the Heaviside step function, and n_0, γ_0, $\hat{\gamma}$, P_0, and V_z are constants. Equilibrium properties are examined in Sec. II, and stability properties are investigated in Secs. III and IV, assuming that $\nu/\hat{\gamma}<<1$, where ν is Budker's parameter.

Introducing the normalized Doppler-shifted eigenfrequency $Z_s=(\omega-kV_z-s\omega_c)/\omega_c$, the TE mode dispersion relation can be expressed as [Eq. (31)],

$$Z_s^3 - \frac{2\nu}{\hat{\gamma}}\,[s/\alpha_{0n}J_2(\alpha_{0n})]^2(Q_sZ_s-s\gamma_z^2\beta_\perp^2H_s)=0 ,$$

where $J_\ell(x)$ is the Bessel function of the first kind of order ℓ, $\omega_c=eB_0/\hat{\gamma}mc$ is the electron cyclotron frequency, k is the axial wavenumber, ω is the complex eigenfrequency, α_{0n} is the nth root of $J_1(\alpha_{0n})=0$, $\beta_\perp^2=(\gamma_0^2-1)/\gamma_0^2$, s=1,2,3,... denotes the magnetic harmonic number, and Q_s and H_s are coupling coefficients [Eq. (27)]. Equation (31) is valid when the group velocity of the vacuum waveguide mode is approximately equal to the beam velocity. Evidently, for given s, the maximum TE mode growth rate occurs at a value of R_0/R_c corresponding to $R_0/R_c=\alpha_{21}/\alpha_{0n}$. Here α_{21} is the first root of $J_2'(\alpha_{21})=0$. This result is different from that obtained for a hollow electron beam.[8-9]

A detailed numerical analysis of the TE mode [Eq. (21)] and TM mode [Eq. (22)] dispersion relations is presented in Sec. IV for the case where the electron gyroradius is much less than the beam radius, i.e., $r_L<<R_0$. Two features are noteworthy from the numerical analysis. First, the system is completely stable to TM mode perturbations when the group velocity of the vacuum waveguide mode is equal to the beam velocity. This appears to be a property unique to the equilibrium distribution function in Eq. (3), where all electrons have the same axial velocity. Second, for TE mode perturbations, the maximum growth rate for a solid beam is comparable to that of a hollow beam. In this context, we conclude that solid relativistic electron beams may also be effective in generating intense microwave radiation by the cyclotron maser instability.

II. EQUILIBRIUM PROPERTIES AND BASIC ASSUMPTIONS

The equilibrium configuration is illustrated in Fig. 1. It consists of an unneutralized electron beam that is infinite in axial extent and propagates parallel to a uniform axial magnetic field $B_0\hat{e}_z$. The radius of the electron beam is denoted by R_0, and a grounded cylindrical conducting wall is located at radius $r=R_c$. The applied magnetic field provides radial confinement of the electrons. As shown in Fig. 1, we introduce a cylindrical polar coordinate system (r,θ,z). In the present analysis, we assume that the beam radius R_0 is larger than twice the thermal electron Larmor radius r_L, i.e., $R_0>2r_L$. It is also assumed that

$$\nu/\hat{\gamma}<<1 \tag{1}$$

where $\nu=N_e e^2/mc^2$ is Budker's parameter,

$$N_e=2\pi\int_0^{R_c} dr\, r\, n_e^0(r) \tag{2}$$

is the number of electrons per unit axial length, $n_e^0(r)$ is the equilibrium electron density, c is the speed of light in vacuo, -e and m are the electron charge and rest mass, respectively, and $\hat{\gamma}mc^2$ is the electron energy in the laboratory frame. The inequality in Eq. (1) indicates that the beam is very tenuous, so that the perturbed fields, to lowest order, can be approximated by the vacuum waveguide fields.[7] Consistent with the low-density assumption in Eq. (1), we also neglect the influence of the (weak) equilibrium self-electric and self-magnetic fields that are produced by the lack of equilibrium charge and current neutralization.

For present purposes, we assume an equilibrium distribution function

of the form,

$$f_e^0(H,P_\theta,P_z) = \frac{n_0}{2\pi\gamma_0 m}\,\delta(H_\perp-\gamma_0 mc^2)\Theta(P_\theta-P_0)\,\delta(P_z-\hat{\gamma}mV_z)\ , \tag{3}$$

where n_0=const. is the electron density at r=0, $\gamma_0 mc^2$ is the electron energy in a frame of reference moving with the mean axial velocity $V_z\hat{e}_z$ of the electron beam,

$$P_0=-(e/2c)(R_0^2-r_L^2)B_0 \tag{4}$$

is the minimum canonical angular momentum of the electrons, and

$$\Theta(x) = \begin{cases} 1\ , & x\geq 0\ , \\ 0\ , & x<0\ , \end{cases} \tag{5}$$

is the Heaviside step function. In Eq. (3),

$$H=\gamma mc^2=(H_\perp^2+c^2p_z^2)^{1/2}=(m^2c^4+c^2p^2)^{1/2} \tag{6}$$

is the total electron energy,

$$P_\theta=[rp_\theta-(e/2c)rB_0] \tag{7}$$

is the canonical angular momentum, and $P_z=p_z$ is the axial canonical momentum, where lower case p denotes mechanical momentum and the equilibrium self fields have been neglected in comparison with the applied magnetic field B_0.

Making use of Eqs. (3) and (4), and defining the effective electron Larmor radius by

$$r_L=(\gamma_0^2-1)^{1/2}c/\hat{\omega}_c, \tag{8}$$

where $\hat{\omega}_c=eB_0/mc$ is the nonrelativistic electron cyclotron frequency, it is straightforward to show that the electron density can be

expressed as

$$n_e^0(r)=n_0\begin{cases} 1\ , & 0<r<R_0-r_L\ , \\ \frac{1}{2}-\frac{1}{\pi}\sin^{-1}\left(\frac{r^2-R_0^2+r_L^2}{2rr_L}\right)\ , & R_0-r_L<r<R_0+r_L\ , \\ 0\ , & \text{otherwise}\ , \end{cases} \tag{9}$$

which is illustrated in Fig. 2. Substituting Eq. (9) into Eq. (2) gives the number of electrons per unit axial length

$$N_e=\pi n_0 R_0^2\ . \tag{10}$$

Note from Eq. (9) that the parameter R_0 introduced in Eq. (4) determines the effective beam radius.

III. LINEARIZED VLASOV-MAXWELL EQUATIONS FOR A TENUOUS BEAM

In this section, we make use of the linearized Vlasov-Maxwell equations to investigate stability properties for azimuthally symmetric perturbations ($\partial/\partial\theta=0$) about a tenuous electron beam equilibrium described by Eq. (3). We adopt a normal-mode approach in which all perturbations are assumed to vary with time (t) and axial coordinate (z) according to

$$\delta\psi(\underset{\sim}{x},t)=\hat{\psi}(r)\exp[i(kz-\omega t)] ,$$

where $\mathrm{Im}\omega>0$, ω is the complex eigenfrequency, and k is the axial wavenumber. Consistent with Eq. (1), it is also valid in lowest order to approximate the perturbed fields by the vacuum waveguide fields.[7,8] Without loss of generality, we assume that the amplitudes of the perturbed axial electric and magnetic fields are normalized according to $\hat{E}_z(r=0)=1$ and $\hat{B}_z(r=0)=1$. After some straightforward algebraic manipulation, we obtain

$$\left(\frac{\omega^2}{c^2}-k^2-\frac{\alpha_{0n}^2}{R_c^2}\right)=-\frac{8\pi\alpha_{0n}/R_c c}{[R_c J_2(\alpha_{0n})]^2}\int_0^{R_c} dr\, r\, J_1(\alpha_{0n}r/R_c)\hat{J}_\theta(r) \qquad (11)$$

for the transverse electric (TE) waveguide modes, and

$$\left(\frac{\omega^2}{c^2}-k^2-\frac{\beta_{0n}^2}{R_c^2}\right)=\frac{8\pi ik}{[R_c J_1(\beta_{0n})]^2}\int_0^{R_c} dr\, r\, J_0(\beta_{0n}r/R_c)\left[\hat{\rho}_e(r)-\frac{\omega}{kc^2}\hat{J}_z(r)\right] \qquad (12)$$

for the transverse magnetic (TM) waveguide modes. [For a detailed derivation of Eqs. (11) and (12), see Ref. 8]. In Eqs. (11) and (12), $J_\ell(x)$ is the Bessel function of first kind of order ℓ, α_{0n} and β_{0n} are the nth roots of $J_1(\alpha_{0n})=0$ and $J_0(\beta_{0n})=0$, and the perturbed charge and current densities are defined by

$$\hat{\rho}_e(r)=-e\int d^3p\ \hat{f}_e(r,\underset{\sim}{p}) \ , \tag{13}$$

and

$$\hat{\underset{\sim}{J}}(r)=-e\int d^3p\ \underset{\sim}{v}\ \hat{f}_e(r,\underset{\sim}{p}) \ , \tag{14}$$

where $\underset{\sim}{v}=\underset{\sim}{p}/(\gamma m)$. The perturbed distribution function in Eqs. (13) and (14) is expressed as

$$\hat{f}_e(r,\underset{\sim}{p})=e\int_{-\infty}^{0} d\tau\ \exp\{i[(kp_z/\gamma m)-\omega]\tau\}\left\{\hat{\underset{\sim}{E}}(r')+\frac{\underset{\sim}{v}'\times\hat{\underset{\sim}{B}}(r')}{c}\right\}\cdot\frac{\partial}{\partial\underset{\sim}{p}'}f_e^0 \ , \tag{15}$$

where $\tau=t'-t$, and the particle trajectories $\underset{\sim}{x}'(t')$ and $\underset{\sim}{p}'(t')$ satisfy $d\underset{\sim}{x}'/dt'=\underset{\sim}{v}'$ and $d\underset{\sim}{p}'/dt'=-e\underset{\sim}{v}'\times B_0\hat{e}_z/c$, with initial conditions $\underset{\sim}{x}'(t'=t)=\underset{\sim}{x}$ and $\underset{\sim}{v}'(t'=t)=\underset{\sim}{v}$. In obtaining Eq. (15), use has been made of the axial orbit

$$z'=z+(p_z/\gamma m)(t'-t) \ .$$

For present purposes it is assumed that

$$|\Omega_s|=|\omega-kV_z-s\omega_c|\ll\omega_c \tag{16}$$

where $\Omega_s=\omega-kV_z-s\omega_c$ is the Doppler-shifted frequency, $\omega_c=eB_0/\hat{\gamma}mc$ is the electron cyclotron frequency in the laboratory frame, and $s=1,2,3,\ldots$ denotes the magnetic harmonic number. To simplify the present analysis, we also assume that

$$\nu/\hat{\gamma}\ll(\beta_\perp\omega_c R_c/c)^2 \ , \tag{17}$$

where $\beta_\perp=(1-1/\gamma_0^2)^{1/2}$. Equation (17) is easily satisfied in parameter regimes of experimental interest.[1-4] Within the context of Eq. (17), it is valid to neglect the terms proportional to $\partial f_e^0/\partial P_\theta$ in Eq. (15), since the corrections associated with these terms are order $(\nu/\hat{\gamma})(c/\beta_\perp\omega_c R_0)^2$ ($\ll1$) or smaller.

The particle trajectories $r'(\tau)$ and $\theta'(\tau)$ in the equilibrium fields are required in order to evaluate the perturbed distribution function in Eq. (15). The transverse (radial and azimuthal) motion of a typical electron is illustrated in Fig. 3(a) for a positive value of canonical angular momentum ($P_\theta>0$), and in Fig. 3(b) for a negative value of canonical angular momentum ($P_\theta<0$). (The dotted circle is the electron orbit in a plane perpendicular to the z-axis). The radial distance of the electron from the z-axis at time $t'=t$ and at $t'=t'$ are denoted by r and r', respectively. The point C is the gyrocenter of the trajectory. The angular coordinates ϕ and ϕ' are the perpendicular velocity-space polar angles at times $t'=t$ and $t'=t'$, and are related by

$$\phi'=\phi+(\hat{\omega}_c/\gamma)(t'-t) \ .$$

The transverse velocities at time $t'=t$ and $t'=t'$ are denoted by $\underset{\sim}{v}_\perp$ and $\underset{\sim}{v}'_\perp$, respectively, and the corresponding speeds are defined by $v_\perp=(v_r^2+v_\theta^2)^{1/2}$ and $v'_\perp=(v_r'^2+v_\theta'^2)^{1/2}$.

The time integration in Eq. (15) can be carried out by making use of the Bessel function summation theorem for the triangles OAB and ABC in Fig. 3. After some straightforward but tedious algebra, the perturbed TE mode distribution function can be expressed as

$$\hat{f}_e^E(r,\underset{\sim}{p}) = \frac{eR_c p_\perp}{\alpha_{0n} cm}\left(\left(\frac{\gamma}{\gamma_0}\,\omega-\frac{kp_z}{\gamma_0 m}\right)\frac{\partial f_e^0}{\partial H_\perp}+k\,\frac{\partial f_e^0}{\partial p_z}\right)\frac{J_s(\alpha_{0n}p_\perp/m\hat{\omega}_c R_c)}{\gamma\omega-s\hat{\omega}_c-kp_z/m}$$

$$\times\sum_{s'=-\infty}^{\infty}(i)^{s'}\exp[is'(\theta-\phi)]\,J_{s'}(\alpha_{0n}r/R_c)\,J_{s+s'}\left(\frac{\alpha_{0n}p_\perp}{m\hat{\omega}_c R_c}\right), \tag{18}$$

and the perturbed TM mode distribution function is given by

$$\hat{f}_e^M(r,p)=e\gamma \frac{\partial f_e^0}{\partial p_z} \frac{J_s(\beta_{0n}p_\perp/m\hat{\omega}_c R_c)}{\gamma\omega-s\hat{\omega}_c-kp_z/m} \sum_{s'=-\infty}^{\infty} (i)^{s'+1}$$

$$\times\exp[is'(\theta-\phi)]J_{s'}(\beta_{0n}r/R_c)J_{s+s'}\left(\frac{\beta_{0n}p_\perp}{m\hat{\omega}_c R_c}\right), \tag{19}$$

where use has been made of $v_\theta'=v_\perp\sin(\phi'-\theta')=(p_\perp/\gamma m)\sin(\phi'-\theta')$ and $p_\perp^2=p_r^2+p_\theta^2$ [For a detailed derivation of Eqs. (18) and (19), the steps are similar to the derivation of Eqs. (38) and (39) in Ref. 8].

In obtaining Eqs. (18) and (19), we have neglected the mode coupling between different values of s, which is consistent with the inequality in Eq. (16). Contributions from the perturbed radial electric field $\hat{E}_r(r)$ have also been neglected in Eq. (19), which is valid provided the group velocity of the vacuum waveguide mode is significantly different from the beam velocity. [For TM mode perturbations, however, it is shown in Sec. IV that the system is stable when the group velocity of the waveguide mode is approximately equal to the beam velocity.]

The equilibrium electron distribution function in Eq. (3) can be expressed as

$$f_e^0 = \frac{n_0}{2\pi m r_L \hat{\omega}_c} \delta(p_\perp-mr_L\hat{\omega}_c)\delta(P_z-\hat{\gamma}m\hat{\omega}_c)\Theta\left(\sin\hat{\phi} - \frac{r^2-R_0^2+r_L^2}{2rr_L}\right) \tag{20}$$

after some simple algebraic manipulation. In Eq. (20), $\hat{\phi}=\phi-\theta$. Substituting Eqs. (18)-(20) into Eq. (11)-(14), and making use of $\hat{\gamma}=\gamma_0(1-V_z^2/c^2)^{-1/2}$ and Eq. (10), we obtain the dispersion relation

$$\left(\frac{\omega^2}{c^2} - k^2 - \frac{\alpha_{0n}^2}{R_c^2}\right) = \frac{4\nu}{\hat{\gamma}R_c^2 J_2(\alpha_{0n})^2}\left\{\frac{(\omega-kV_z)Q_s(\alpha_{0n}R_0/R_c,\alpha_{0n}r_L/R_c)}{\omega-kV_z-s\omega_c}\right.$$

$$\left. - \frac{(\omega^2-k^2c^2)H_s(\alpha_{0n}R_0/R_c,\ \alpha_{0n}r_L/R_c)\beta_\perp^2}{(\omega-kV_z-s\omega_c)^2}\right\} \tag{21}$$

for TE mode perturbations, and

$$\left(\frac{\omega^2}{c^2} - k^2 - \frac{\beta_{0n}^2}{R_c^2}\right) = \frac{4\nu K_s(\beta_{0n}R_0/R_c, \beta_{0n}r_L/R_c)}{\hat{\gamma}R_c^2 J_1(\beta_{0n})^2} \left\{\frac{\omega - kV_z}{\omega - kV_z - s\omega_c} - \frac{(kc - \omega V_z/c)^2}{(\omega - kV_z - s\omega_c)^2}\right\} \tag{22}$$

for TM mode perturbations. In Eqs. (21) and (22), $\beta_\perp = r_L\hat{\omega}_c/c$, $\nu = N_e e^2/mc^2$ is Budker's parameter, and the coupling coefficients H_s, Q_s, and K_s are defined by

$$\begin{aligned}
H_s(x,y) &= (1-y/x)^2 J_2(x-y)^2 J_s'(y)^2 + 2J_s'(y) I_s^E(x,y) \ , \\
Q_s(x,y) &= 2(1-y/x)^2 J_2(x-y)^2 [J_s'(y)^2 + yJ_s'(y)J_s''(y)] \\
&\quad + 2[2J_s'(y) + yJ_s''(y)] I_s^E(x,y) + yJ_s'(y)[I_{s-1}^E(x,y) \\
&\quad - I_{s+1}^E(x,y)] \ , \\
K_s(x,y) &= (1-y/x)^2 J_1(x-y)^2 J_s(y)^2 + J_s(y) I_s^M(x,y) \ ,
\end{aligned} \tag{23}$$

where the prime (') denotes d/dy. The integrals I_s^E and I_s^M in Eq. (23) are defined by

$$\begin{aligned}
I_s^E(x,y) &= -\frac{1}{2\pi x^2} \int_{x-y}^{x+y} du\, u\, J_1(u) \int_{\hat{\phi}_0}^{\pi-\hat{\phi}_0} d\hat{\phi} \sin\hat{\phi} J_s[(u^2+y^2-2uy\sin\hat{\phi})^{1/2}] \\
&\quad \times \exp\left\{ i s \cos^{-1}\left[\frac{y - u\sin\hat{\phi}}{(u^2+y^2-2uy\sin\hat{\phi})^{1/2}}\right]\right\} \ , \\
I_s^M(x,y) &= \frac{1}{\pi x^2} \int_{x-y}^{x+y} du\, u\, J_0(u) \int_{\hat{\phi}_0}^{\pi-\hat{\phi}_0} d\hat{\phi}\, J_s[(u^2+y^2-2uy\sin\hat{\phi})^{1/2}] \\
&\quad \times \exp\left\{ i s \cos^{-1}\left[\frac{y - u\sin\hat{\phi}}{(u^2+y^2-2uy\sin\hat{\phi})^{1/2}}\right]\right\} \ ,
\end{aligned} \tag{24}$$

where

$$\hat{\phi}_0 = \sin^{-1}\left(\frac{u^2+y^2-x^2}{2uy}\right) . \tag{25}$$

For the case of small thermal electron Larmor radius,

$$r_L/R_0 << 1, \tag{26}$$

the terms proportional to I_ℓ^E and I_ℓ^M in Eq. (23) are negligible in comparison with other terms. We, therefore, approximate Eq. (23) by

$$\begin{aligned} H_s(x,y) &= J_2(x)^2 J_s'(y)^2 \ , \\ Q_s(x,y) &= 2J_2(x)^2 [J_s'(y)^2 + yJ_s'(y)J_s''(y)] \ , \\ K_s(x,y) &= J_1(x)^2 J_s(y)^2 \ . \end{aligned} \tag{27}$$

For a specified value of Budker's parameter $(\nu/\hat{\gamma})$ and perpendicular beam energy, it is evident from Eq. (27) that the coupling coefficient between the vacuum waveguide mode and the electron cyclotron resonance mode $(\omega = kV_z + s\omega_c)$ is a maximum when $J_2'(\alpha_{0n}R_0/R_c)=0$ for the TE mode, and when $J_1'(\beta_{0n}R_0/R_c)=0$ for the TM mode. In this context, we conclude that the maximum coupling for magnetic harmonic number s occurs for a value of R_0/R_c given by

$$R_0/R_c = \begin{cases} \alpha_{21}/\alpha_{0n} \ , & \text{TE mode} \ , \\ \alpha_{11}/\beta_{0n} \ , & \text{TM mode} \ , \end{cases} \tag{28}$$

where α_{21} and α_{11} are the first roots of $J_2'(\alpha_{21})=0$ and $J_1'(\alpha_{11})=0$, respectively. Note from Eq. (28) that the value of R_0/R_c corresponding to maximum coupling is the same for <u>all</u> magnetic harmonic numbers, which is remarkably different from the results previously obtained[8,9] for a hollow electron beam, where the maximum TE mode coupling coefficient is proportional to $J_s(\alpha_{s1})^2$. As shown in Eq. (27), the maximum TE mode coupling coefficient for a solid beam is proportional to $J_2(\alpha_{21})^2$. Therefore, for purposes of producing intense microwave radiation, it appears that a solid electron beam may be as effective as a hollow beam. In the following section, the dispersion relations

in Eqs. (21) and (22) are solved numerically for the case of small thermal Larmor radius, with $r_L/R_0 \ll 1$.

IV. STABILITY ANALYSIS

In this section, the linear dispersion relations in Eqs. (21) and (22) are solved numerically for $r_L << R_0$. For the TE mode dispersion relation [Eq. (21)], we assume that the group velocity of the vacuum waveguide mode is approximately equal to the beam velocity,[8] i.e.,

$$V_g = \frac{kc^2}{\omega} \simeq V_z \ . \tag{29}$$

Making use of the TE vacuum waveguide mode dispersion relation, $\omega^2/c^2-k^2=\alpha_{0n}^2/R_c^2$, the cyclotron resonance condition, $\omega=kV_z+\omega_c$, and Eq. (29), we obtain the lowest-order solution

$$\begin{aligned} \omega_0 &= \gamma_z^2 s\omega_c \ , \\ k_0 &= \gamma_z^2 \beta_z s\omega_c/c \ , \\ R_c &= \alpha_{0n} c/\gamma_z s\omega_c \ , \end{aligned} \tag{30}$$

for microwave generation at frequency $\omega=\gamma_z^2 s\omega_c$. Here $\gamma_z^2=(1-\beta_z^2)^{-1}$ and $\beta_z=V_z/c$. Substituting Eq. (30) into Eq. (21) and iterating, we obtain the approximate TE mode dispersion relation

$$Z_s^3 - \frac{2\nu}{\hat{\gamma}} \left(\frac{s}{\alpha_{0n} J_2(\alpha_{0n})} \right)^2 [Q_s(x,y) Z_s - s\gamma_z^2 \beta_\perp^2 H_s(x,y)] = 0 \ , \tag{31}$$

where the normalized Doppler-shifted eigenfrequency Z_s is defined by $Z_s=(\omega-kV_z-s\omega_c)/\omega_c$, Q_s and H_s are defined in Eq. (27), and $x=\alpha_{0n}R_0/R_c$ and $y=\alpha_{0n}r_L/R_c=\gamma_z s\beta_\perp$. Since the electron beam is assumed to satisfy $R_0>2r_L$ (see Sec. II), the allowable range of R_0/R_c is restricted to $R_0/R_c>2\gamma_z s\beta_\perp/\alpha_{0n}$, where use has been made of Eq. (29). [Therefore, in Fig. 4 the growth rate plots are presented only for values of $R_0/R_c>2\gamma_z s\beta_\perp/\alpha_{0n}$.]

Shown in Fig. 4 are plots of normalized growth rate $Im\omega/\omega_c=\omega_i/\omega_c$ versus R_0/R_c obtained from Eq. (31) (TE mode) for $\nu=0.001$, $\beta_\perp=0.4$, $\beta_z=0.3$, and several values of (s,n). Several features are noteworthy from Fig. 4. First, the maximum growth rate for each set of (s,n) occurs at the value of R_0/R_c given by $R_0/R_c=\alpha_{21}/\alpha_{0n}$. Second, the general shape of the growth rate curve is similar in form to that obtained for s=2 perturbations about a hollow electron beam. [See Fig. 7 of Ref. 8.] Third, the maximum growth rate for the solid beam configuration considered here is comparable to the maximum growth rate for a hollow beam.[8] In this context, we conclude that the cyclotron maser instability in a solid beam may also be an effective means for generating intense microwave radiation.

We now investigate a typical example that illustrates the dependence of TM mode stability behavior on k. Figure 5 shows a plot of normalized growth rate $Im\omega/\omega_c=\omega_i/\omega_c$ versus normalized axial wavenumber kc/ω_c obtained from Eqs. (22) and (27) for $\nu=0.001$, $R_0/R_c=0.5$, $r_L/R_c=0.1$, $\beta_z=0.3$, n=2 and several values of s. It is evident from Fig. 5 and Eq. (22) that the growth rate vanishes at $k=k_0=\gamma_z^2\beta_z s\omega_c/c$, which is identical to the condition in Eq. (29). We therefore conclude that the system is completely stable to TM mode perturbations when the group velocity of the vacuum waveguide mode is equal to the beam velocity. This appears to be a unique property of the equilibrium distribution function in Eq. (3), where all electrons have the same axial velocity. It is important to note, however, that the TM mode growth rate can be substantial for axial wavenumbers different from $\gamma_z^2\beta_z s\omega_c/c$.

V. SUMMARY AND CONCLUSIONS

In this paper, we have examined the cyclotron maser instability for an intense solid electron beam propagating parallel to a uniform axial guide field. The analysis was carried out within the framework of the linearized Vlasov-Maxwell equations. The equilibrium (Sec. II) and cyclotron maser stability (Secs. III and IV) properties were investigated in detail for the choice of distribution function in which all electrons have the same value of perpendicular energy, the same value of axial velocity, and a step-function distribution in canonical angular momentum. One of the most important conclusions of this study is that the maximum instability growth rate for a solid electron beam is comparable to that of a hollow beam. Moreover, it is also found that the maximum growth rate for magnetic harmonic number s occurs at a value of R_0/R_c corresponding to $R_0/R_c = \alpha_{21}/\alpha_{0n}$ for TE mode perturbations, and $R_0/R_c = \alpha_{11}/\beta_{0n}$ for TM mode perturbations. For the TM mode, however, the growth rate vanishes when the group velocity of the vacuum waveguide mode is equal to the beam velocity. In this context, the TE mode is more effective at producing intense microwave radiation in a solid beam than the TM mode.

ACKNOWLEDGMENTS

This research was supported by the National Science Foundation. The research by one of the authors (H.S.U.) was supported in part by the Office of Naval Research under the auspices of the University of Maryland-Naval Research Laboratory Joint Program in Plasma Physics.

REFERENCES

1. J. L. Hirshfield, I. B. Bernstein, and J. M. Wachtel, IEEE J. Quantum Electronics, Vol. QE-1, 237 (1965).
2. V. L. Granatstein, P. Sprangle, R. K. Parker, J. Pasour, M. Herndon, and S. P. Schlesinger, Phys. Rev. A14, 1194 (1976).
3. N. I. Zaytsov, T. B. Pankratova, M. I. Petelin, and V. A. Flyagin, Radio Engineering and Electronics Physics 19, 103 (1974).
4. D. V. Kisel, G. S. Korablev, V. G. Navelyeu, M. I. Petelin, and Sh. E. Tsimring, Radio Engineering and Electronic Physics 19, 95 (1974).
5. P. Sprangle and A. Drobot, IEEE Trans. MTT-25, 528 (1977).
6. V. A. Flyagin, A. V. Gaponov, M. I. Petelin, and V. K. Yulpatov, IEEE Trans. MTT-25, 514 (1977).
7. H. Uhm, R. C. Davidson, and K. R. Chu, Phys. Fluids, in press (1978).
8. H. Uhm, R. C. Davidson, and K. R. Chu, Phys. Fluids, in press (1978).
9. K. R. Chu, "Theory of Electron Cyclotron Maser Interactions in a Cavity at the Harmonic Frequencies", submitted for publication (1978).

FIGURE CAPTIONS

Fig. 1 Equilibrium configuration and coordinate system.

Fig. 2 Electron density profile [Eq. (9)].

Fig. 3 Electron orbit for (a) $P_\theta > 0$, and (b) $P_\theta < 0$ projected on a plane perpendicular to the z-axis.

Fig. 4 Plots of normalized TE mode growth rate ω_i/ω_c versus R_0/R_c [Eq. (31)] for $\nu=0.001$, $\beta_\perp=0.4$, $\beta_z=0.3$, and several values of (s,n).

Fig. 5 Plots of normalized TM mode growth rate ω_i/ω_c versus kc/ω_c [Eq. (22)] for $\nu=0.001$, $n=2$, $\beta_z=0.3$, $R_0/R_c=0.5$, $r_L/R_c=0.1$, and several values of s.

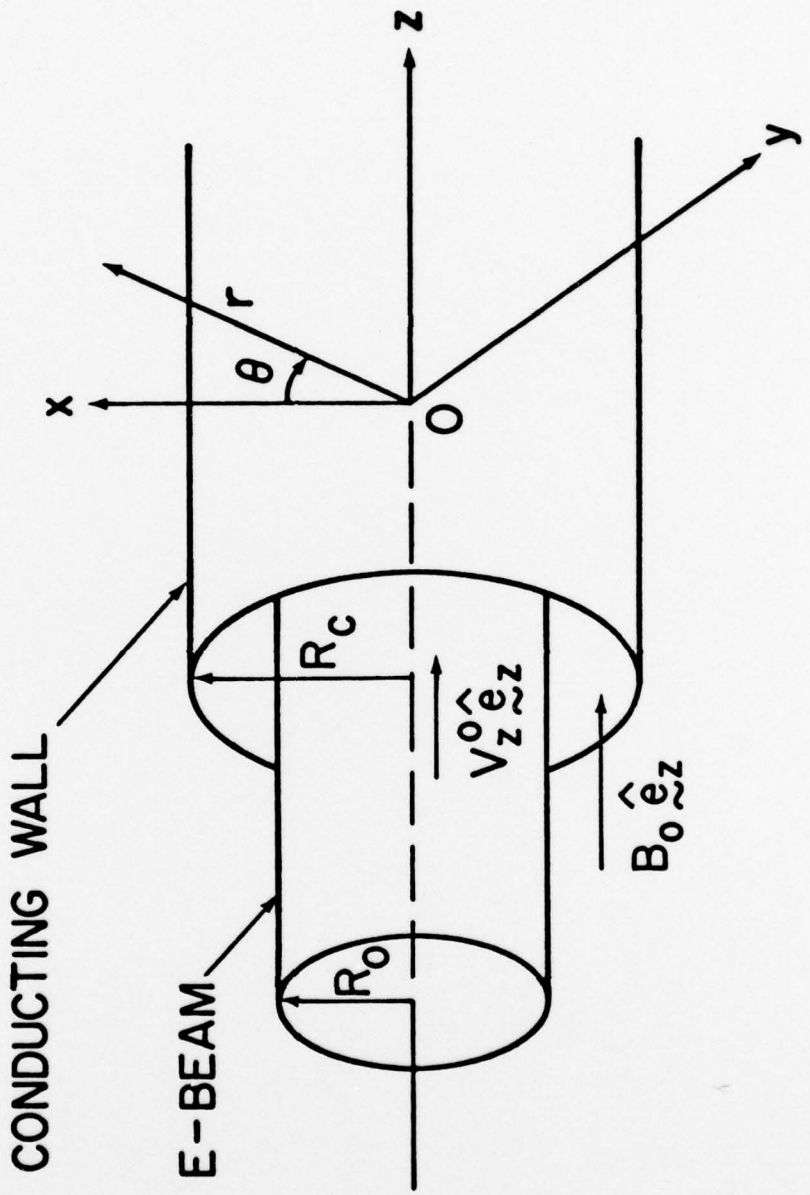

Fig. 1

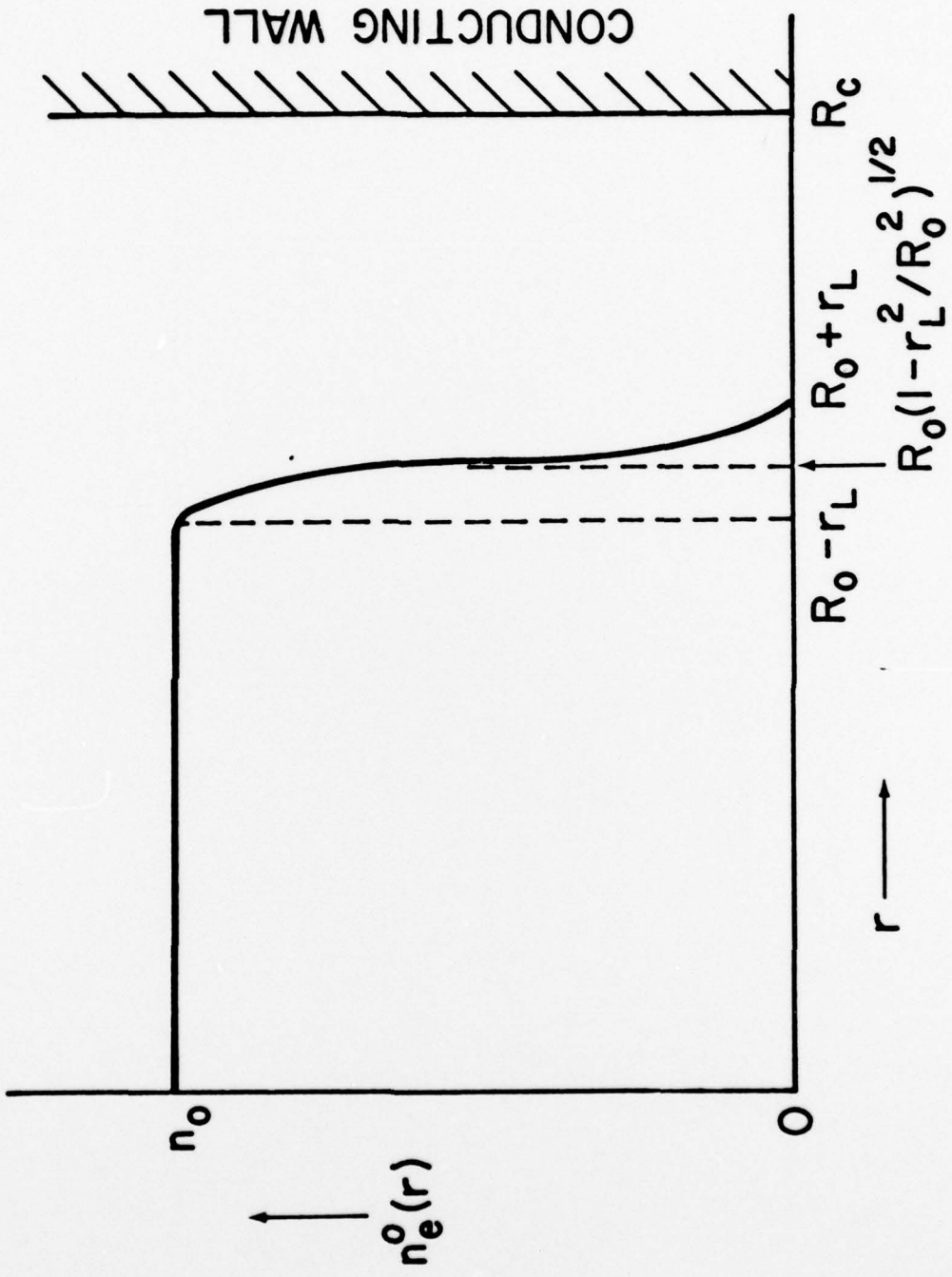

Fig. 2

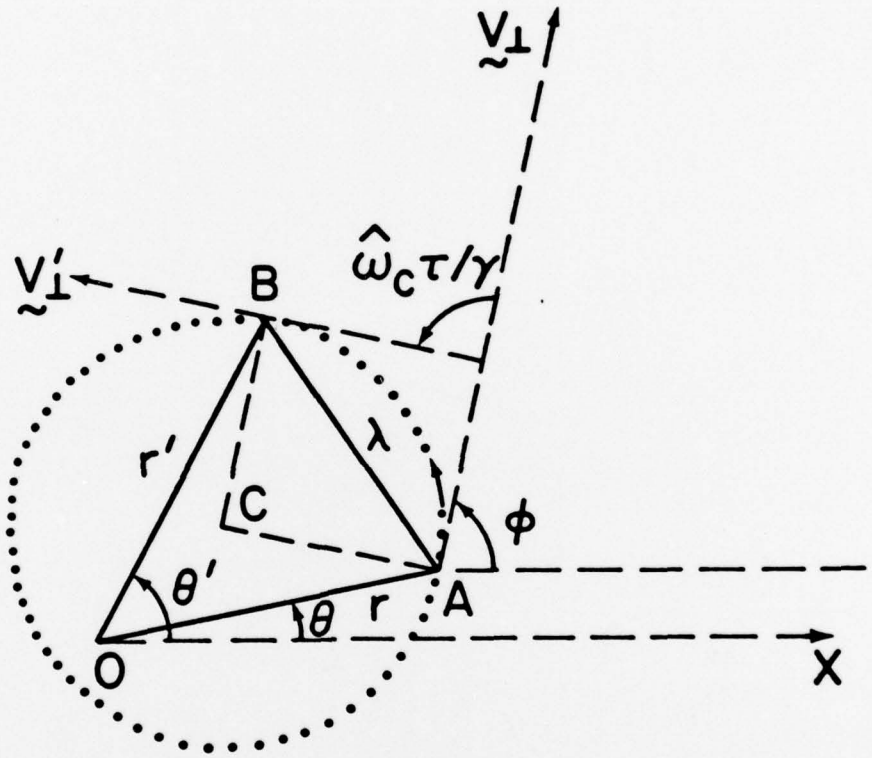
$\underset{\sim}{V}_\perp$
$\hat{\omega}_c\tau/\gamma$
$\underset{\sim}{V}'_\perp$
B
r'
λ
C
φ
θ'
θ
r
A
O
X

Fig. 3a

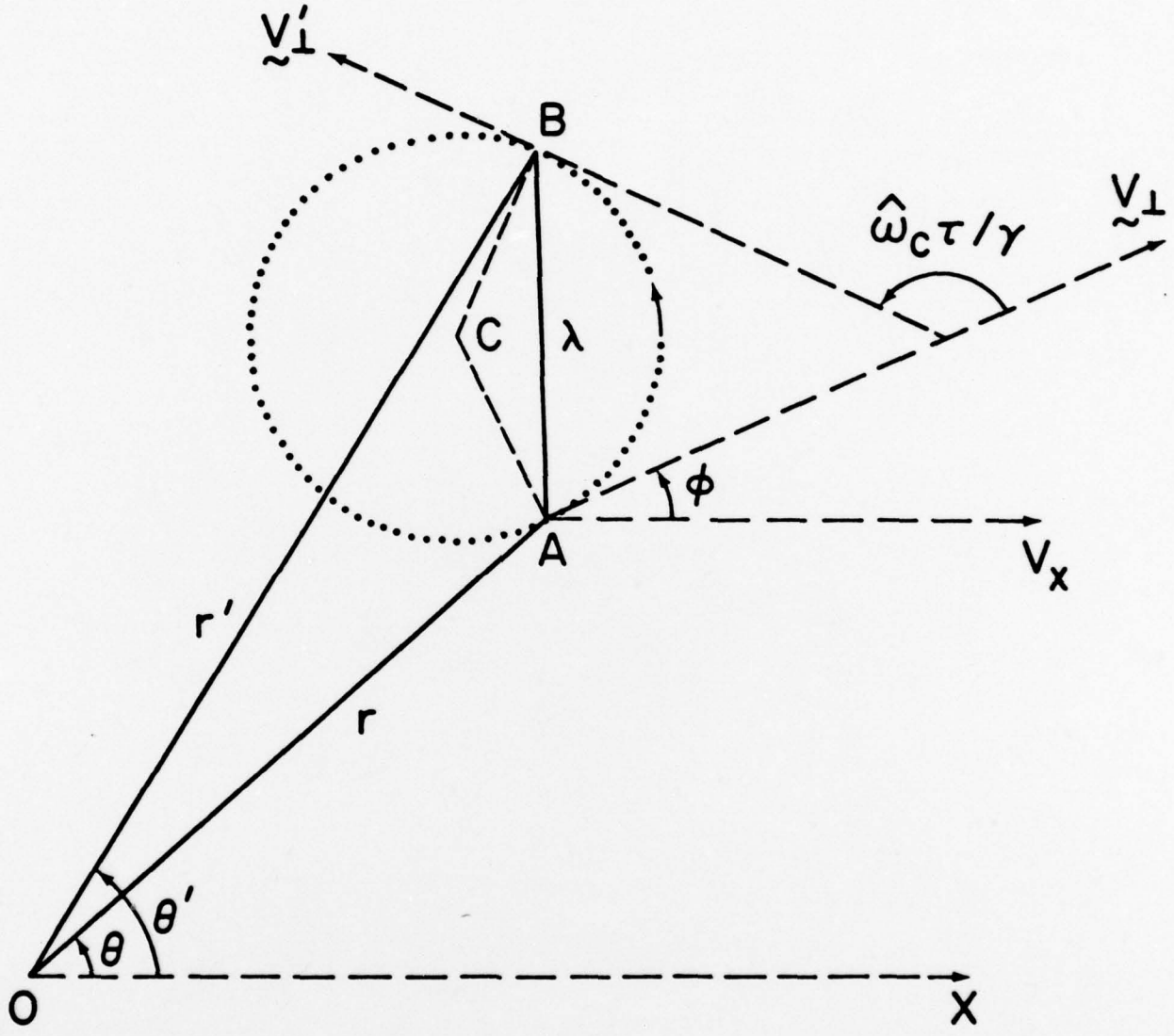

Fig. 3b

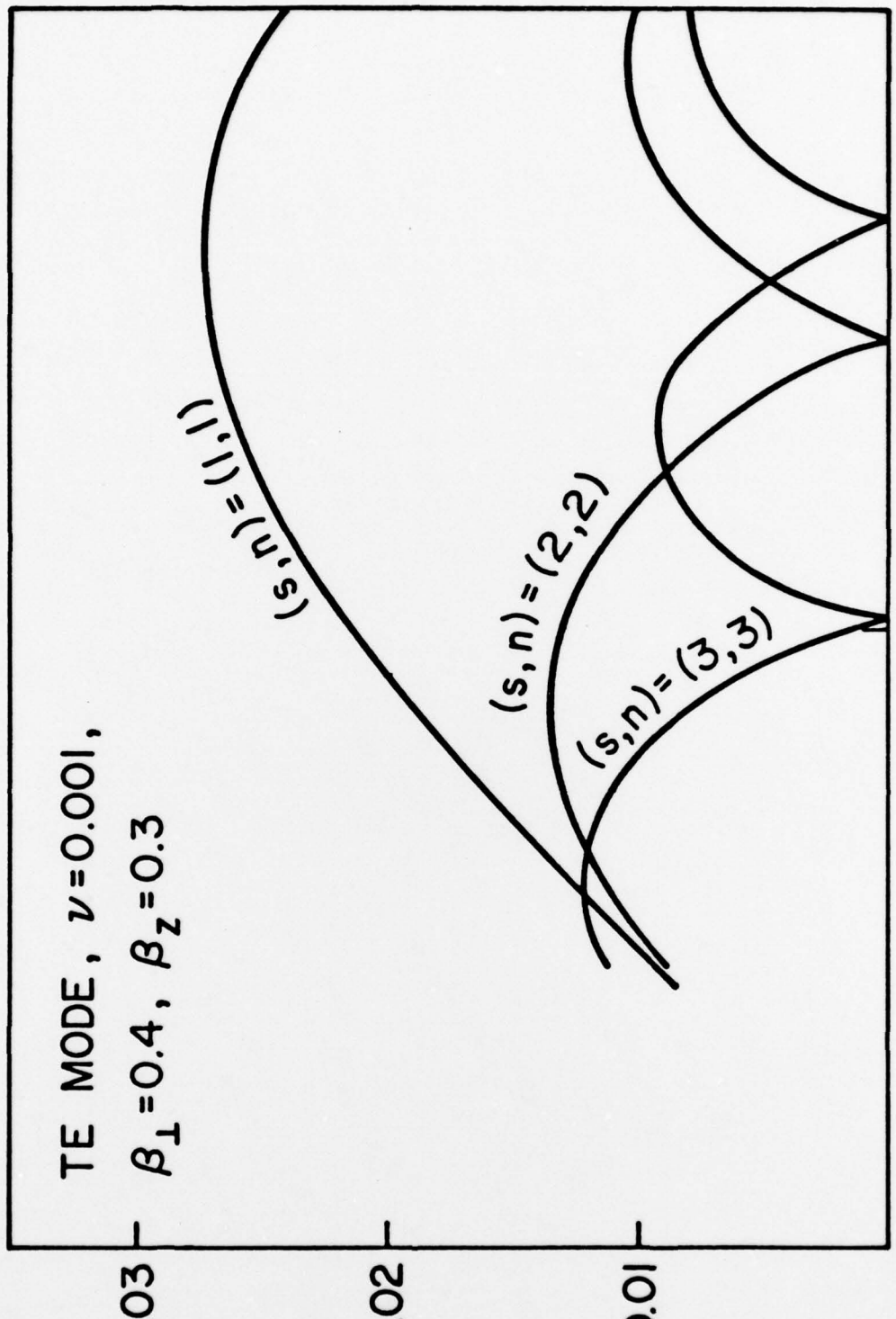
TE MODE, ν=0.001,
$\beta_\perp$=0.4, β_z=0.3
(s,n)=(1,1)
(s,n)=(2,2)
(s,n)=(3,3)
0.03
0.02
0.01
0.0
0.5
1.0
$\frac{\omega_i}{\omega_c}$
R_o/R_c

Fig. 4

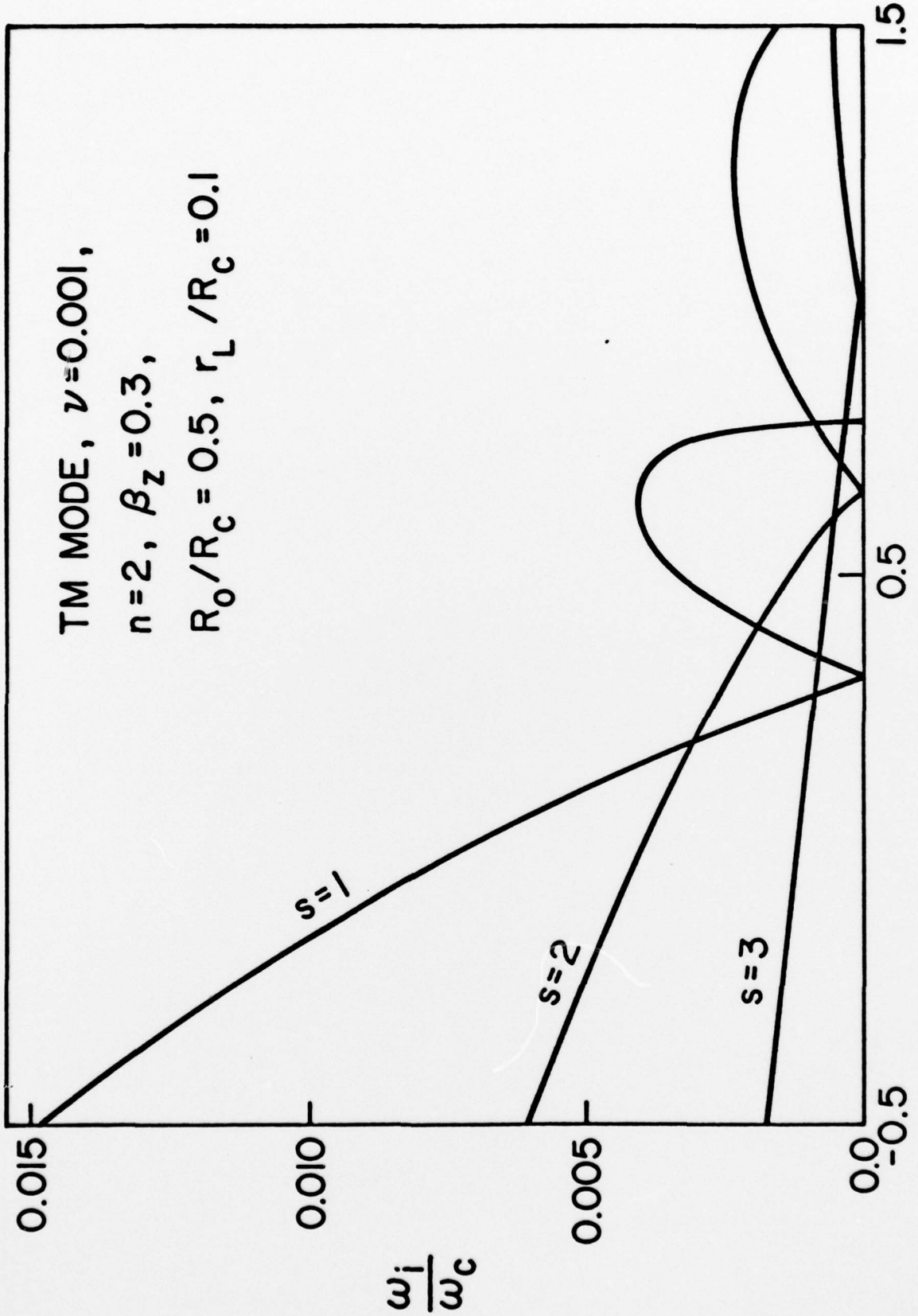
TM MODE, ν=0.001,
n=2, β_z=0.3,
R_0/R_c = 0.5, r_L /R_c =0.1
s=1
s=2
s=3
0.015
0.010
0.005
0.0
-0.5
0.5
1
1.5
ω_i/ω_c
kc/ω_c

Fig. 5